DOI: 10.1002/adma.201803477
Article type: Communication

Title Rhenium doped and stabilized MoS_2 atomic layers with basal plane catalytic activity

Shi-Ze Yang, Yongji Gong, Priyanka Manchanda, Yu-Yang Zhang, Gonglan Ye, Shuangming Chen, Li Song, Sokrates T. Pantelides, Pulickel M. Ajayan,* Matthew F. Chisholm, Wu Zhou**

Dr. Shi-Ze Yang, Prof. Sokrates T. Pantelides, Dr. Matthew F. Chisholm, Prof. Wu Zhou
Materials Science and Technology Division, Oak Ridge National Laboratory, Oak Ridge, Tennessee 37831, USA

Prof. Yongji Gong
School of Materials Science & Engineering, Beihang University, Beijing 100191, China.
E-mail: yongjigong@buaa.edu.cn

Prof. Yongji Gong, Dr. Gonglan Ye, Prof. Pulickel M. Ajayan
Department of Materials Science & NanoEngineering, Rice University, Houston, Texas 77005, USA
Email: ajayan@rice.edu

Dr. Priyanka Manchanda, Prof. Yu-Yang Zhang, Prof. Sokrates T. Pantelides
Department of Physics and Astronomy, Vanderbilt University, Nashville, Tennessee 37235, USA

Prof. Yu-Yang Zhang, Prof. Wu Zhou
School of Physical Sciences and CAS Center for Excellence in Topological Quantum Computation, University of Chinese Academy of Sciences, Beijing 100049, China
Email: wuzhou@ucas.ac.cn

Dr. Shuangming Chen, Prof. Li Song
National Synchrotron Radiation Laboratory, CAS Center for Excellence in Nanoscience, University of Science and Technology of China, Hefei, Anhui 230029, China

Keywords: transition metal dichalcogenides, hydrogen evolution reaction, electrocatalysis, scanning transmission electron microscopy, density functional theory

Abstract.

The development of stable and efficient hydrogen evolution reaction (HER) catalysts is essential for the production of hydrogen as a clean energy resource. A combination of experiment and theory demonstrates that the normally inert basal planes of 2D layers of MoS_2 can be made highly catalytically active for the HER when alloyed with rhenium (Re). The presence of Re at the ~50% level converts the material to a stable distorted tetragonal (DT) structure that shows enhanced HER activity as compared to most of the MoS_2-based catalysts reported in the literature. More importantly, this new alloy catalyst shows much better stability over time and cycling than lithiated 1T-MoS_2. Density functional theory (DFT) calculations find that the role of Re is only to stabilize the DT structure, while catalysis occurs primarily in local Mo-rich DT configurations, where the HER catalytic activity is very close to that in Pt. The study provides a new strategy to improve the overall HER performance of MoS_2-based materials via chemical doping.

Main Text Paragraphs.

Creating fuel from water is a dream solution to the global problem of increasing energy demand. Producing improved electrocatalysts is critical to achieving this goal. Platinum (Pt) offers the best catalytic performance for hydrogen evolution reaction (HER), but it is expensive. Several possible candidates including transition metal sulfides and phosphides have been developed as catalysts for HER to replace Pt.[1-8] Among them, molybdenum disulfide (MoS_2) is a cheap and abundant mineral with its edge structure closely resembling that of hydrogen-producing enzymes found in nature.[2, 9] While the edge sites of MoS_2 show high activity for HER, the basal plane of the room-temperature stable 2H-phase MoS_2 is catalytically inert.[9-10] Several strategies have been proposed to enhance the activity of MoS_2, including preparing nanostructures,[2, 11-12] enhancing defect concentration,[13-16] introducing a degree of disorder and oxygen incorporation[17], and doping with transition metal atoms,[18-21] such as Pt at the 1-2% level.[21] Among those efforts, it has been shown that alkaline metal intercalation can transform MoS_2 into a metallic tetragonal phase (T-phase) in which the basal plane

becomes active for hydrogen production.[22-25] Lithium intercalated T-phase MoS_2, thus, has been considered as a benchmark for the evaluation of HER catalytic activity of MoS_2 based catalysts. However, the bonding between alkaline atoms and MoS_2 is very weak, and T-phase MoS_2 easily transforms back into the stable and less active 2H-phase. Therefore, new methods to produce highly stable and active HER catalysts based on MoS_2 are of fundamental importance and explored herein.

Because the H-to-T phase transformation of MoS_2 via lithium intercalation has been proposed to be an electronic effect,[26] doping MoS_2 with metals that have a different number of valence electrons than Mo may serve as an alternative way to produce stable T-phase MoS_2 to activate the basal plane. Rhenium (Re) has a similar radius as Mo but has one more valence electron. In addition, ReS_2 is a stable layered material with a distorted tetragonal (DT) structure and has the same chemical stoichiometry as MoS_2. Moreover, Re metal is also active for HER.[27-28] Thus, we expected that alloys of $(Re,Mo)S_2$ would form a stable T-phase structure with high HER performance.

Herein, we demonstrate that stable T-phase MoS_2 can be obtained by alloying with Re. The stable structure changes from the hexagonal phase of pure MoS_2 to a DT phase when the Re content is >50%. The HER performance was found to be optimized in the 50% Re-50% Mo $(Re,Mo)S_2$ alloy. This alloy was found to have enhanced HER activity with a low onset potential of 90 mV and a small Tafel slope of 56 mV/dec, as well as excellent stability. Density functional theory (DFT) calculations of phase stability confirmed the DT structure observed in $Re_xMo_{1-x}S_2$ alloys with Re concentration larger than 50%. Theoretically calculated hydrogen adsorption energies were found to be as low as 0.06 eV for the active Mo-rich sites in the 50% Re-50% Mo alloy. It is noteworthy that the role of Re is only to convert the 2H-phase to the stable DT-phase while catalytic activity decreases with Re concentrations higher than ~50%. Our results provide a new design strategy to enhance the electrocatalytic activity of 2D transition-metal dichalcogenides for H_2 production while maintaining their high chemical stability. Two-dimensional (2D) $Re_xMo_{1-x}S_2$ flakes were grown on Si/SiO_2 wafers using chemical vapor deposition (CVD). The morphology and composition of the flakes produced with different precursor amounts were determined (**Figure S1**, S2 and Table S1). The samples are primarily monolayer, with a

small fraction of few-layer regions. In particular, we use annular dark-field (ADF) imaging in a scanning transmission electron microscope (STEM) to provide direct maps of the atom distributions in the 2D layers and to quantify the local composition with single-atom sensitivity (Figure 1).[29] Structural models highlighting only the metal atoms (Re and Mo) are shown in Figure 1 (structural models with sulfur sites included can be found in Figure S3). A histogram of the observed cation site intensities revealed two distinct peaks that correspond to Re and Mo occupation, respectively (Figure S4). We observed that only a small amount of Re (2% to 4%) is incorporated in the H-phase MoS_2. The Re content in the DT structures was found to be controllable between 55% and 100% in the four different high Re-content samples. Statistical analysis of cation metal atom distributions (Figure S5) shows that Re and Mo atoms in these layers are randomly distributed. No enrichment of dopants along the edges was observed (Figure S6).

As a 2D layer, pure MoS_2 is hexagonal (H phase, point group D_{3h}) while pure ReS_2 has a distorted tetragonal (DT, point group C_i) structure (Figure 2a and 2b) at ambient conditions. These materials consist of a plane of transition metal atoms sandwiched between two chalcogen atomic planes. The DT structure of ReS_2 contains parallel strings of Re atoms in rhombic arrangement (Figure 2b and 2d), and the slightly wider separation between the strings generates lower contrast in the ADF images, seen as darker channels. Sulfur atoms located within the strings (darker yellow, Figure 2b) have shorter metal-sulfur bonds as compared to those of sulfur atoms in the channels (yellow, Figure 2b). As will be discussed later, the different bonding environments of the S atoms in the DT structure have profound influence on the HER activity of the basal plane.

Similar to the phase transformation for lithium intercalated MoS_2, the 1H- to DT- phase transition for Re-doped MoS_2 can be explained by crystal field theory.[30] For 1H-MoS_2, in which Mo atoms occupy trigonal prismatic sites, the lowest energy level (d_{z^2} orbital) is fully occupied by the electrons of Mo atoms. When there are extra electrons due to Re doping, the extra electrons fill higher energy levels (d_{xy} and $d_{x^2-y^2}$ orbitals) which destabilize the system (see Figure S7 for a pictorial representation). This destabilization can also be inferred from Figure 2c as the calculated mixing energy of the H-

phase $Re_xMo_{1-x}S_2$ alloy increases with increasing Re content. In contrast, transition metal atoms are octahedrally coordinated in the DT structure. Three of the five *d* orbitals sit at a lower energy level which can accommodate more electrons. This structure, therefore, becomes more stable with increasing Re content. A transition from the 1H structure to the DT structure is predicted to be more energetically favorable when the Re/(Re+Mo) concentration is greater than ~50% (Figure 2c), which is in agreement with the experimental observation as shown in Figure 1.

Electrochemical measurements were systematically carried out to evaluate the HER performance of the $Re_xMo_{1-x}S_2$ alloy samples. Figure 3a−3c show the polarization curves (linear sweep voltammetry), Tafel plots and extracted parameters of three $Re_xMo_{1-x}S_2$ alloy samples and four control samples, including Pt, pure 2H-MoS_2, pure DT-ReS_2 and lithium intercalated 1T-MoS_2. The $Re_{0.55}Mo_{0.45}S_2$ alloy sample with the DT structure is superior to any of the MoS_2–based samples tested, showing a low onset potential of 90 mV and a Tafel slope of 56 mV/dec. Both its overpotential and Tafel slope show improvements over those for the metallic 1T-MoS_2, which was widely considered as the most promising catalyst to replace Pt for HER. In addition, this performance is also superior to that of other MoS_2-based catalysts with well-engineered defects or morphologies (Figure S8, S9 and Table S2).[12-13, 15, 31-32] We evaluated the active site density from STEM images (Figure S10) and calculated the turn-over frequency (TOF) to further understand the intrinsic performance of the $Re_{0.55}Mo_{0.45}S_2$ alloy sample. The TOF value of the $Re_{0.55}Mo_{0.45}S_2$ alloy sample was calculated to be 3.48 S^{-1} and 0.015 S^{-1} at overpotentials of 300 mV and 0 mV, respectively. These values are superior to those of the edge/defect engineered MoS_2 samples with 0.725 S^{-1} at 300 mV and 0.013 S^{-1} at 0 mV.[13, 32]

Stability of the catalytic performance over time and cycling is another main factor to evaluate the performance of catalysts. The instability of lithiated 1T-MoS_2 has been limiting its general applicability as an HER catalyst,[22] since it reverts to 2H-MoS_2 over time or cycling, leading to drastic decrease of catalytic performance. HER stability tests were carried out on the $Re_{0.55}Mo_{0.45}S_2$ alloy sample and lithiated 1T-phase MoS_2. HER performance was measured after one, two, and six months of storage in air under ambient conditions. The overpotential (at current density of 10 mA/cm^2) of the

$Re_{0.55}Mo_{0.45}S_2$ alloy sample started at 0.169 V for the fresh sample and increased to 0.174 V after 1 month, 0.176 V after 2 months, and 0.177 V after 6 months, *i.e.* with a total increase of about 5% over 6 months (Figure 4a). In sharp contrast, the overpotential (at current density of 10 mA/cm^2) of the lithiated 1T-phase MoS_2 control sample increased by over 120% after only two months of storage. Cycling experiments were also carried out for up to 3,000 cycles. The overpotential (at current density of 10 mA/cm^2) for the $Re_{0.55}Mo_{0.45}S_2$ alloy was found to increase by only 2 mV after 3,000 sweeping cycles, whereas the overpotential (at current density of 10 mA/cm^2) of lithium intercalated 1T- MoS_2 was nearly doubled to a value of 0.378 V after 3,000 cycles (Figure 4c and 4d). Ex-situ Raman spectroscopy was used to probe the possible structural changes after reaction. The sharp Raman peaks associated with the DT structure were still present after 3,000 sweeping cycles (Figure S11), demonstrating that the DT structure was well maintained. All results indicate that the DT-phase $Re_{0.55}Mo_{0.45}S_2$ alloy is not only catalytically more active than the 1T-phase MoS_2 but also much more stable. The high catalytic activity and the superior stability of the DT-phase $Re_{0.55}Mo_{0.45}S_2$ alloy make it a much more promising catalyst for practical HER application than the benchmark lithiated 1T MoS_2.

Systematic density functional theory (DFT) calculations were performed in order to identify the catalytically active site structures responsible for the high HER activity in the DT-phase $Re_{0.55}Mo_{0.45}S_2$ catalyst. It is well-accepted that a good indicator for evaluating an HER catalyst is that the Gibbs free energy (ΔG_H) for hydrogen adsorption should be close to zero,[2] which means hydrogen atoms can get access to and desorb from the catalyst surface easily. The calculated ΔG_H values for a pristine basal plane of 1H-MoS_2 and DT-ReS_2 are 2.1 eV and 1.44 eV, respectively, in agreement with earlier findings,[15] indicating that the basal plane sites in both 1H-MoS_2 and DT-ReS_2 are inactive. For comparison, the calculated ΔG_H values for the basal plane of T-MoS_2 and Pt (111) surface are only 0.13 eV and 0.02 eV,[33] respectively, consistent with their good HER activities observed experimentally.

We then calculated ΔG_H for different atomic sites in the Re-doped MoS_2 monolayers in order to investigate their corresponding HER performance. In light of the experimental results, we considered a

DT phase $Re_xMo_{1-x}S_2$ alloy monolayer with the Re positions extracted from the experimental STEM-ADF image of $Re_{0.55}Mo_{0.45}S_2$ (Figure 5a). Typical sites for hydrogen adsorption were evaluated as shown in Figure 5a. It was found that ΔG_H depends strongly on the local bonding environment in the DT phase $Re_xMo_{1-x}S_2$ alloy monolayer (see Figure S12 and Table S3). As mentioned earlier (Figure 2d), there are two types of sulfur atoms in the DT structure: those located inside the narrow metal strings and those in the wider channels between the strings. It is important to note that S atoms located inside the narrow metal strings have an average metal-S bond length of 2.38 Å, whereas S atoms in the channels have a longer average metal-S bond length of 2.48 Å. We find that S sites in the wider channels (see Sites 1-4 in Figure S12 and Table S3) are generally more active as compared to the S sites located inside the strings (Sites 5-8 in Figure S12 and Table S3). *The most active S site is surrounded by three Mo atoms with the longest Mo-S bond lengths* (labeled as Site-1 in Figure 5a), with ΔG_H of 0.06 eV. In contrast, S atoms located within the strings with shorter metal-sulfur bonds are less active. In addition, ΔG_H also depends on the type of metal atoms bonded to the S sites. Increasing the number of Re atoms surrounding the S atoms shortens the Re-S bond lengths and decreases the HER activity (Figure S12 and Table S3). The least active site S atom is located in the string and surrounded by three Re atoms with short Re-S bond lengths, labeled as Site-8 in Figure 5 with a ΔG_H of 1.36 eV.

It was demonstrated that an increase in HER activity is typically correlated with an increase in the density of states near the Fermi energy.[15] Figure 5b shows the projected density of states (DOS) of S atoms for the most active and the least active sites, respectively (Site-1 and Site-8 in Figure 5a). Indeed, we find that the S atom at Site-1 has more states near the Fermi energy than the S atom at Site-8. It is clear that the presence of the extra states in the vicinity of the Fermi energy is correlated with the longer Mo-S bond lengths.

The theoretical results discussed above indicate that the most active sites are S atoms in the Mo enriched wider channels in $Re_{0.55}Mo_{0.45}S_2$, which can be viewed as local DT-phase MoS_2. This stable local DT-phase MoS_2 is achieved in $Re_xMo_{1-x}S_2$ alloy monolayers with Re concentration above ~50%.

It should be noted, however, that the role of Re is only to convert the H-phase into a stable DT phase, while its presence actually degrades the catalytic activity by forming shorter Re-S bonds that deplete the catalytically-active states near the Fermi energy. An increase of the Re concentration above 55%, while still resulting in the DT-phase structure, yields a lower percentage of the most active Mo-rich local DT-MoS_2 structure and consequently a decrease in the overall HER activity. Additional calculations involving edge structures did not produce activity better than those obtained in the $Re_{0.55}Mo_{0.45}S_2$ basal plane (Figure S13 and S14).[2, 34] As a result, $Re_{0.5}Mo_{0.5}S_2$ is catalytically more active as compared to the samples with higher concentrations of Re, as observed experimentally in Figure 3. The net conclusion is that ~50% Re doping of MoS_2 leads to stable patches of DT-MoS_2, which exhibit superior HER catalytic activity.

To summarize, a highly stable DT-structured $Re_xMo_{1-x}S_2$ alloy catalyst ($Re_{0.55}Mo_{0.45}S_2$) was prepared with superior HER performance. In particular, this material has a higher catalytic activity and much better stability than the benchmark lithium intercalated 1T-MoS_2. DFT calculations of the change in Gibbs free energy associated with hydrogen adsorption indicate that the basal plane of the DT-structured alloy catalyst is active. Specifically, the relatively wide channels between cation chains in the DT structure, locally enriched with Mo atoms, provide the most active sites with hydrogen adsorption energies as low as 0.06 eV. The strong bonding between sulfur and metal atoms keeps the structure stable during the HER reaction. Although Re is not an inexpensive metal, our results suggest that MoS_2-based catalysts can be further improved by alloying with an element that induces a stable T-phase structure while simultaneously activating the basal plane. Further exploration of other metal dopants having a different number of valence electrons than Mo, such as Mn or Nb, may potentially lead to new MoS_2-based catalysts and move the HER performance of these materials even closer to that obtained with Pt.

Supporting Information

Supporting Information is available from the Wiley Online Library or from the author.

Acknowledgements

W.Z. and Y.Y.Z. acknowledge support from the Natural Science Foundation of China (51622211), the CAS Pioneer Hundred Talents Program and Key Research Program of

Frontier Sciences, CAS. Y.G. acknowledges support from the National Key R&D Program of China (Grant No. 2018YFA0306900). The electron microscopy (S.Z.Y., M.F.C. and W.Z.) was supported in part by the U.S. Department of Energy, Office of Science, Basic Energy Sciences, Materials Science and Engineering Division and through a user proposal supported by ORNL's Center for Nanophase Materials Sciences, which is sponsored by the Scientific User Facilities Division of U.S. Department of Energy. Work at Vanderbilt (P.M., Y.Y.Z. and S.T.P.) was supported by the U.S. Department of Energy under grant DE-FG02-09ER46554 and by the McMinn Endowment. Computational resources were provided by the National Energy Research Scientific Computing Center (NERSC), a DOE Office of Science User Facility supported by the Office of Science of the U.S. Department of Energy under Contract No. DE-AC02-05CH11231, and the Extreme Science and Engineering Discovery Environment (XSEDE), which is supported by National Science Foundation Grant ACI-1053575. Y.G. and W.Z. conceived the idea and designed the experiments. Y.G., G.Y. and P.M.A. performed material growth and electrochemical measurements. S.Z.Y., M.F.C. and W.Z. performed electron microscopy of the materials. P.M., Y.Y.Z. and S.T.P. performed DFT calculations. S. C. and L. S. carried out the X-ray absorption spectroscopy. W.Z., S.Z.Y., Y.G., P.M. and M.F.C. wrote the manuscript. All authors discussed the results and commented on the manuscript. S.Z.Y, Y.G. and P.M. contributed equally to this work.

Received: ((will be filled in by the editorial staff))
Revised: ((will be filled in by the editorial staff))
Published online: ((will be filled in by the editorial staff))

References

[1] X. Zou, Y. Zhang, *Chem. Soc. Rev.* **2015,** *44*, 5148.
[2] B. Hinnemann, P. G. Moses, J. Bonde, K. P. Jørgensen, J. H. Nielsen, S. Horch, I. Chorkendorff, J. K. Nørskov, *J. Am. Chem. Soc.* **2005,** *127*, 5308.
[3] X. Chia, A. Y. S. Eng, A. Ambrosi, S. M. Tan, M. Pumera, *Chem. Rev.* **2015,** *115*, 11941.
[4] M. Chhowalla, H. S. Shin, G. Eda, L.-J. Li, K. P. Loh, H. Zhang, *Nat. Chem.* **2013,** *5*, 263.
[5] D. J. Li, U. N. Maiti, J. Lim, D. S. Choi, W. J. Lee, Y. Oh, G. Y. Lee, S. O. Kim, *Nano Lett.* **2014,** *14*, 1228.
[6] Y. Shi, B. Zhang, *Chem. Soc. Rev.* **2016,** *45*, 1529.
[7] E. J. Popczun, C. G. Read, C. W. Roske, N. S. Lewis, R. E. Schaak, *Angew. Chem., Int. Ed.* **2014,** *53*, 5427.
[8] E. J. Popczun, J. R. Mckone, C. G. Read, A. J. Biacchi, A. M. Wiltrout, N. S. Lewis, R. E. Schaak, *J. Am. Chem. Soc.* **2013,** *135*, 9267.
[9] T. F. Jaramillo, K. P. Jørgensen, J. Bonde, J. H. Nielsen, S. Horch, I. Chorkendorff, *Science* **2007,** *317*, 100.
[10] W. Jaegermann, H. Tributsch, *Prog. Surf. Sci.* **1988,** *29*, 1.
[11] Z. Chen, D. Cummins, B. N. Reinecke, E. Clark, M. K. Sunkara, T. F. Jaramillo, *Nano Lett.* **2011,** *11*, 4168.
[12] H. Wang, Z. Lu, D. Kong, J. Sun, T. M. Hymel, Y. Cui, *ACS Nano* **2014,** *8*, 4940.
[13] J. Xie, H. Zhang, S. Li, R. Wang, X. Sun, M. Zhou, J. Zhou, X. W. Lou, Y. Xie, *Adv. Mater.* **2013,** *25*, 5807.
[14] G. Ye, Y. Gong, J. Lin, B. Li, Y. He, S. T. Pantelides, W. Zhou, R. Vajtai, P. M. Ajayan, *Nano Lett.* **2016,** *16*, 1097.
[15] H. Li, C. Tsai, A. L. Koh, L. Cai, A. W. Contryman, A. H. Fragapane, J. Zhao, H. S. Han, H. C. Manoharan, F. Abild-Pedersen, J. K. Norskov, X. Zheng, *Nat. Mater.* **2016,** *15*, 48.

[16] C. Tsai, H. Li, S. Park, J. Park, H. S. Han, J. K. Norskov, X. Zheng, F. Abild-Pedersen, *Nat. Commun.* **2017,** *8*, 15113.
[17] J. Xie, J. Zhang, S. Li, F. Grote, X. Zhang, H. Zhang, R. Wang, Y. Lei, B. Pan, Y. Xie, *J. Am. Chem. Soc.* **2013,** *135*, 17881.
[18] H. Wang, C. Tsai, D. Kong, K. Chan, F. Abild-Pedersen, J. K. Nørskov, Y. Cui, *Nano Res.* **2015,** *8*, 566.
[19] J. V. Lauritsen, F. Besenbacher, *J. Catal.* **2015,** *328*, 49.
[20] J. V. Lauritsen, S. Helveg, E. Lægsgaard, I. Stensgaard, B. S. Clausen, H. Topsøe, F. Besenbacher, *J. Catal.* **2001,** *197*, 1.
[21] J. Deng, H. Li, J. Xiao, Y. Tu, D. Deng, H. Yang, H. Tian, J. Li, P. Ren, X. Bao, *Energy Environ. Sci.* **2015,** *8*, 1594.
[22] S. S. Chou, N. Sai, P. Lu, E. N. Coker, S. Liu, K. Artyushkova, T. S. Luk, B. Kaehr, C. J. Brinker, *Nat. Commun.* **2015,** *6*, 8311.
[23] X. Geng, W. Sun, W. Wu, B. Chen, A. Al-Hilo, M. Benamara, H. Zhu, F. Watanabe, J. Cui, T.-P. Chen, *Nat. Commun.* **2016,** *7*, 10672.
[24] M. A. Lukowski, A. S. Daniel, F. Meng, A. Forticaux, L. Li, S. Jin, *J. Am. Chem. Soc.* **2013,** *135*, 10274.
[25] D. Voiry, M. Salehi, R. Silva, T. Fujita, M. Chen, T. Asefa, V. B. Shenoy, G. Eda, M. Chhowalla, *Nano Lett.* **2013,** *13*, 6222.
[26] M. Py, R. Haering, *Can. J. Phys.* **1983,** *61*, 76.
[27] R. Garcia-Garcia, G. Ortega-Zarzosa, M. Rincón, G. Orozco, *Electrocatalysis* **2015,** *6*, 263.
[28] S. Trasatti, *J. Electroanal. Chem. Interfacial Electrochem.* **1972,** *39*, 163.
[29] Y. Gong, Z. Liu, A. R. Lupini, G. Shi, J. Lin, S. Najmaei, Z. Lin, A. L. Elías, A. Berkdemir, G. You, H. Terrones, M. Terrones, R. Vajtai, S. T. Pantelides, S. J. Pennycook, J. Lou, W. Zhou, P. M. Ajayan, *Nano Lett.* **2014,** *14*, 442.
[30] X. Sun, Z. Wang, Z. Li, Y. Q. Fu, *Sci. Rep.* **2016,** *6*, 26666.
[31] J. H. Lee, W. S. Jang, S. W. Han, H. K. Baik, *Langmuir* **2014,** *30*, 9866.
[32] D. Kong, H. Wang, J. J. Cha, M. Pasta, K. J. Koski, J. Yao, Y. Cui, *Nano Lett.* **2013,** *13*, 1341.
[33] E. Skulason, G. S. Karlberg, J. Rossmeisl, T. Bligaard, J. Greeley, H. Jonsson, J. K. Norskov, *Phys. Chem. Chem. Phys.* **2007,** *9*, 3241.
[34] A. Bruix, H. G. Füchtbauer, A. K. Tuxen, A. S. Walton, M. Andersen, S. Porsgaard, F. Besenbacher, B. Hammer, J. V. Lauritsen, *ACS Nano* **2015,** *9*, 9322.

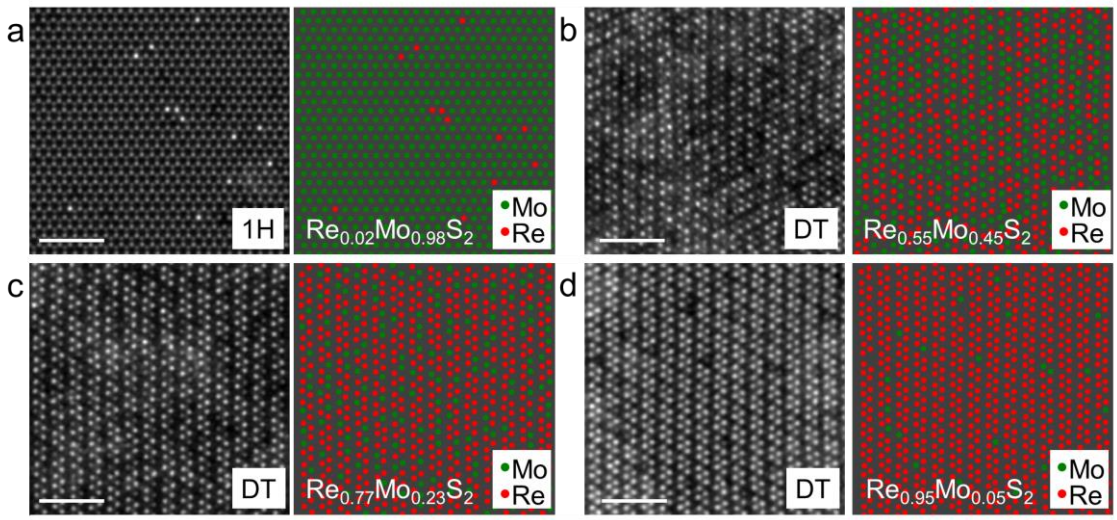

Figure 1. Structure of $Re_xMo_{1-x}S_2$ alloy monolayers at different Re concentrations. a-d, Experimental STEM-ADF images (left) paired with the corresponding atom mapping images (right). The Re and Mo atoms are identified by image intensities. S atoms are omitted from the atom mapping images for clarity. Re concentrations are determined directly from the atom mapping image. Scale bars: 2 nm.

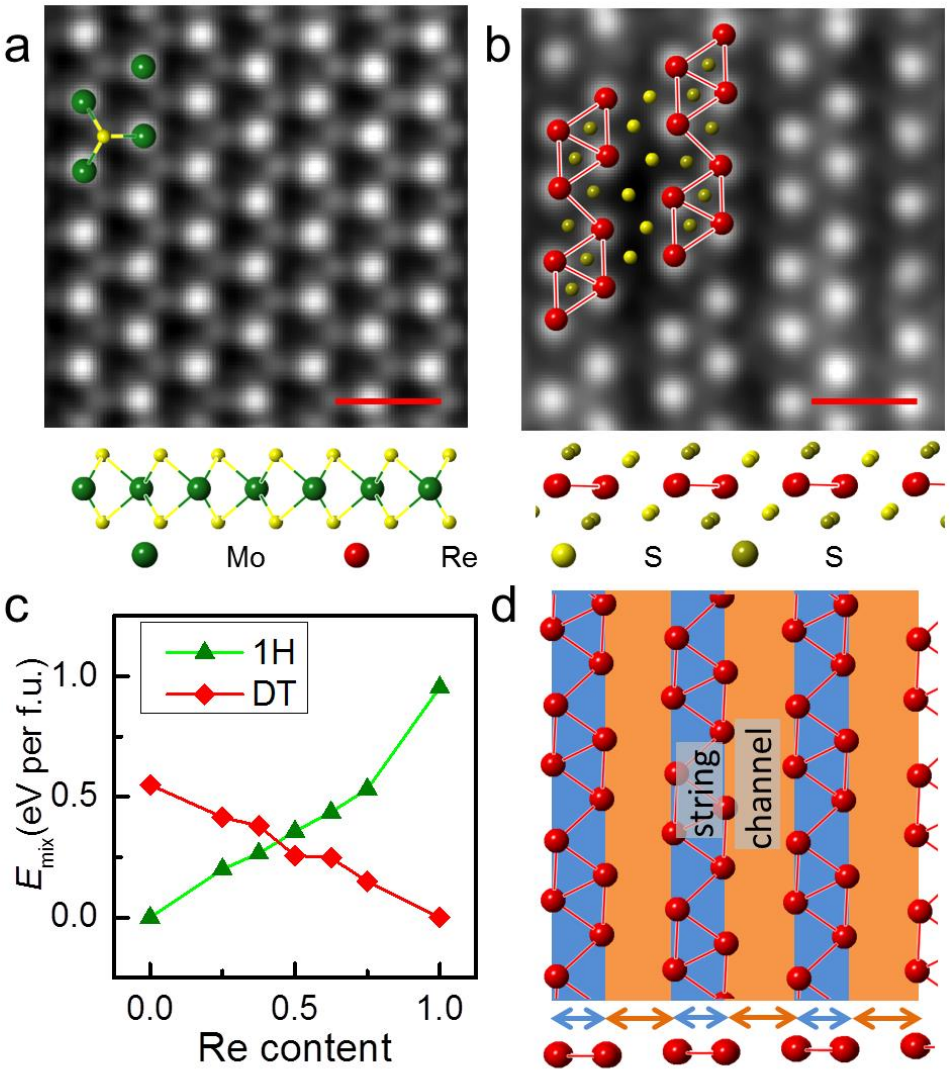

Figure 2. 1H and DT structures and their enthalpy of mixing at different Re concentrations. a, b, STEM-ADF images of monolayers of 1H MoS_2 (a) and DT ReS_2 (b). The structural models are overlaid on the ADF images with Mo atoms in green, Re atoms in red; S atoms in the wider channels are in yellow and S atoms in the strings of Re are in darker yellow. Side views of the structural models are shown in the lower panels. Scale bars: 0.5 nm. c, Calculated mixing energy in 1H and DT phase $Re_xMo_{1-x}S_2$ alloy at different Re concentrations. d, Schematic showing the metal atoms in the DT structure. The metal rhombic strings are shown in blue and are separated by the slightly wider channels shown in orange.

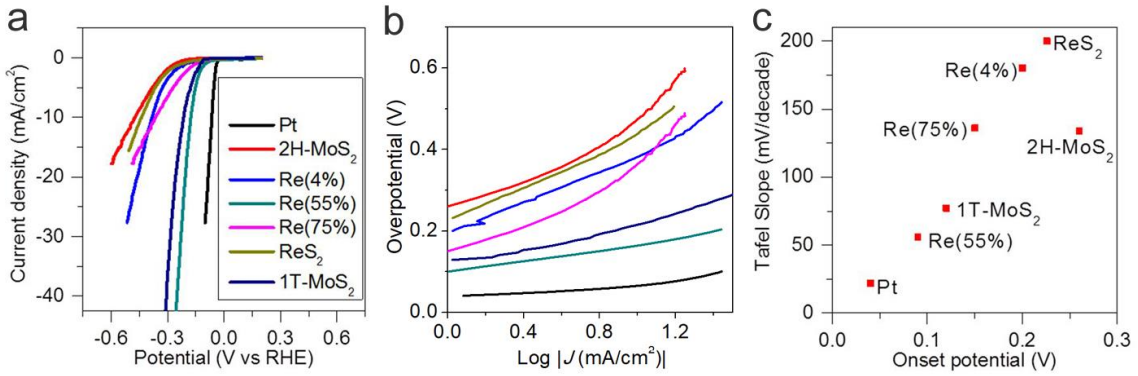

Figure 3. Electrocatalytic performance of different Re-doped MoS_2 catalysts and reference samples. a, Polarization curves of different samples. b, Tafel plots of different Re-doped MoS_2 catalysts and reference samples, derived from the polarization curves shown in a. c, Tafel slope and onset overpotentials.

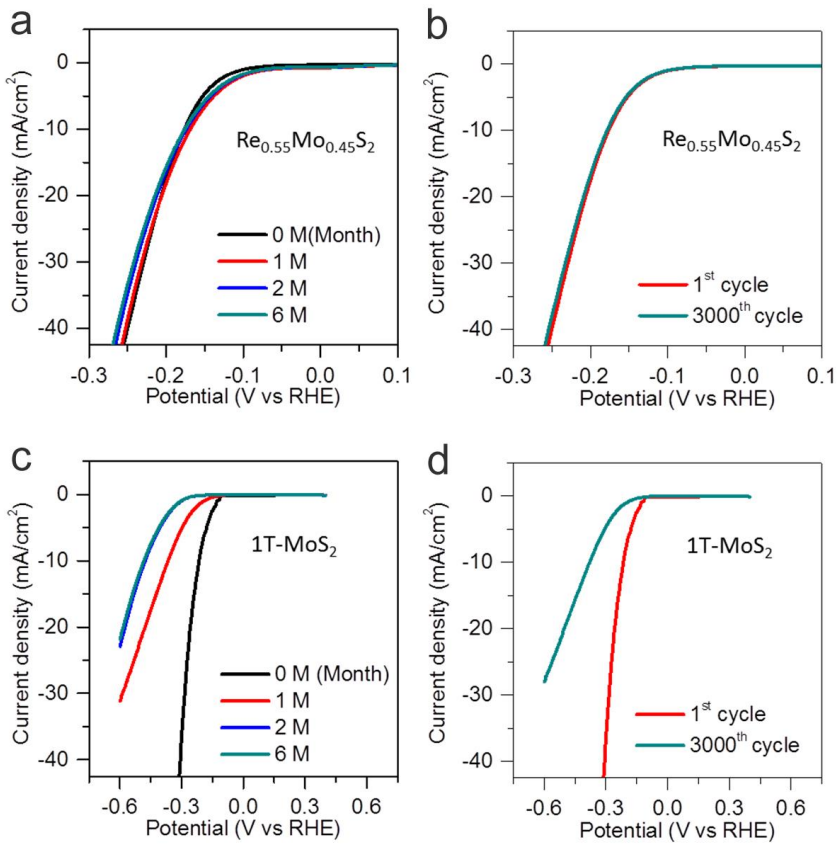

Figure 4. Stability test of $Re_{0.55}Mo_{0.45}S_2$ alloy and 1T-MoS_2 over time and cycling. a, Polarization curves of the $Re_{0.55}Mo_{0.45}S_2$ alloy sample, measured after one, two, and six months of storage in air under ambient conditions. b, Cycling test of the $Re_{0.55}Mo_{0.45}S_2$ alloy sample. Polarization curves for the first cycle and 3000th cycle are shown. c, Polarization curves of lithium intercalated 1T-MoS_2, measured after one, two, and six months of storage under ambient conditions. d, Cycling test of lithium intercalated 1T-MoS_2 sample. Polarization curves for the first cycle and 3000th cycle show significant loss of catalytic performance.

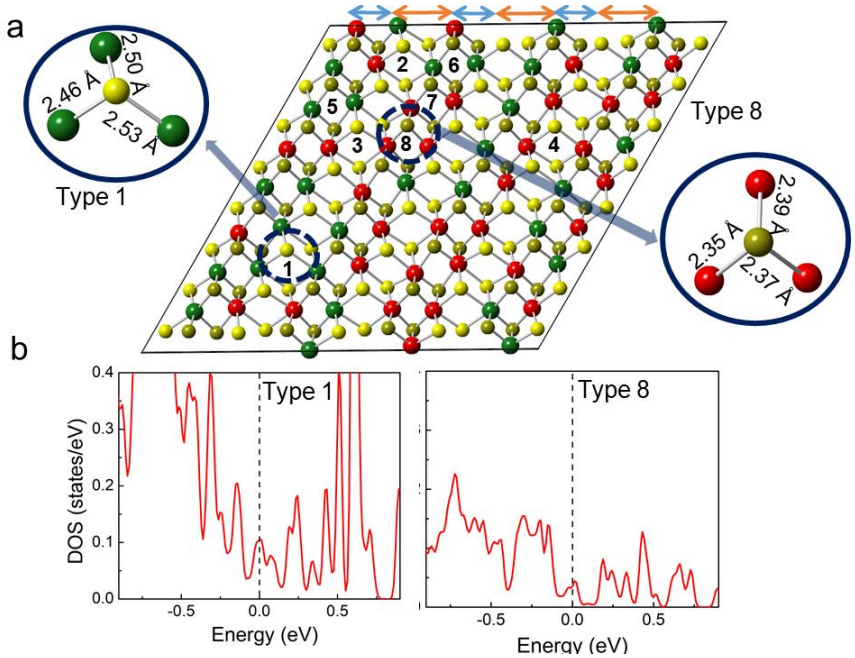

Figure 5. Local bonding environment and electronic structure of the active sites in the DT $Re_xMo_{1-x}S_2$ alloy. a, Structural model of a DT phase $Re_xMo_{1-x}S_2$ alloy monolayer with randomly distributed Re atoms. Mo atoms in green, Re atoms in red and S atoms in yellow. The strings and channels are identified with blue and orange arrows, respectively. S atom bonded with three Mo atoms in between two metal rhombic strings (zoomed-in view of Site 1) serves as the most active site, while S bonded with three Re atoms within the metal strings (zoomed-in view of Site 8) is the least active site. b, Projected density of states of the most active and the least active sites, respectively.